Cornelia Wenger*, Andreas Fellner, Fred Bucek, Paul Werginz, Frank Rattay

Simulating auditory nerve fiber response following micro-electrode stimulation

Comparing efficiency of electrode placements in the scala tympani and scala vestibuli

https://doi.org/10.1515/cdbme-2023-1202

Abstract: The cochlear implant was the first effective and is still the most common neuroprosthetic device which is employed for people with severe to profound hearing loss. To restore auditory perception, an array of micro-electrodes that deliver electrical pulses to the auditory nerve is surgically implanted into the lower cochlea duct, the scala tympani (ST). However, implantation into the upper cavity, the scala vestibuli (SV) has been tested due to severe anatomical obstruction or ossification of the ST. Clinical results revealed similar performance and thresholds for SV and ST cochlear implant users. We present a simulation study of auditory nerve fibre response to monophasic stimulation of both polarities. Excitation profiles are compared for micro-electrodes placed in the SV and equivalent positions in the ST. In total, 7 different electrode positions for 4 different fibres have been investigated in a homogenous 2D model. Results for the intact fibres predict generally higher anodic thresholds in comparison to cathodic stimulation at the same electrode position and mostly lower thresholds for the SV electrodes in comparison to their ST counterparts. In contrast, anodic thresholds are mostly lower than cathodic thresholds for the degenerated fibres. Furthermore, due to the increased electrode-fibre distance for degenerate fibres which have completely lost the dendrite, SV stimulation is less beneficial. However, for basal fibres and the clinically relevant mid scala placement of the electrode the typically high thresholds remain similar for ST and SV positions.

Keywords: auditory nerve fibres, extracellular stimulation, excitation patterns, cochlear implants, scala vestibuli.

***Corresponding author: Cornelia Wenger:** Vienna University of Technology, Institute for Analysis and Scientific Computing, Wiedner Hauptstraße 8-10, 1040, Vienna, Austria, e-mail: cornelia.wenger@asc.tuwien.ac.at

Andreas Fellner, Fred Bucek, Frank Rattay: Vienna University of Technology, Institute for Analysis and Scientific Computing, Vienna, Austria

Paul Werginz: Vienna University of Technology , Institute of Biomedical Electronics, Vienna, Austria

1 Introduction

The spiral-shaped cochlea plays a key role in the sense of hearing. It contains 3 fluid-filled chambers (Figure 1 left): ST, SV and the scala media (SM). When sound waves enter the cochlea the resulting fluid movement causes the sensory hearing cells to bend, converting mechanical forces into electrical signals which are transferred to the brain via auditory nerve fibres (ANFs). These ANFs are tonotopically arranged, i.e., the ANFs are spiralled up along the cochlea which correspond to decreasing specific frequencies from base (20kHz) to apex (200Hz) in order to decode sound.

A cochlear implant (CI) consists of an implanted electrode array that stimulates ANFs to initiate nerve signals in people with severe to profound hearing loss with one million estimated users globally [1]. Traditionally the CI electrode array is inserted into the ST. CI candidates often show cochlear obstruction due to ossification, post-meningitis fibrosis, etc. In the ST, specifically the basal turn, this block impedes full electrode insertion which reduces low frequency perception. As an alternative, electrode insertion into the non-obstructed SV has already been tested in 1990 [2]. It was speculated that a larger electrode distance to the soma of ANFs may be a disadvantage for SV implantation. However, a following comprehensive clinical study predicted equivalent performance between ST and SV CI users and a potential advantage for speech recognition in noisy environments for SV implantation [3]. A recent study confirmed full SV insertion and predicted electrical stimulation of neuronal elements across all frequencies [4].

We present a first exploratory computational study which aims to investigate the electrode placement in SV and ST. The excitation pattern including thresholds and initiation sites are compared in four ANFs for different electrode positions: 3 equivalent positions in SV and ST and 1 additional ST position. With a 2D model, we are able to confirm previously reported trends for pulse polarity of extracellular stimulation in healthy and completely degenerated ANFs. Furthermore, obtained results predict that excitation patterns are comparable for equivalent ST and SV electrode positions.

2 Materials and Methods

Four realistic ANF pathways have been manually placed at appropriate positions in a human cochlea based on a photograph adapted from [5] (Figure 1). ANF1 and ANF2 belong to the basal turn whereas ANF3 and ANF4 are from the middle turn of the cochlea. The soma positions and resulting lengths of the two processes have been extracted. Subsequently, the typical structure of the human ANF was implemented onto selected pathways: The peripheral process (dendrite, diameter d=1.3µm) starts with a terminal (PTerm), then consists of an alternating sequence of internodes (PI) and nodes of Ranvier (PN) and ends with a pre-somatic area (PAIS). Due to the varying length of the dendrites, ANF2 has five internodes and all other ANFs have six. Simulations of the completely degenerated ANF omit the whole dendrite. After the spherical soma (d=20µm), the central process (d=2.6µm) also has a post-somatic area (CAIS) and an alternating sequence of internodes (CI) and nodes (CN).

In order to study the initiation and propagating of an action potential (AP) the spatial and temporal changes in transmembrane voltage have to be calculated for each of the connected section. Then the total current in the *n*-th section is composed of transmembrane and axial currents to its neighbours. Each subunit consists of a capacitive and resistive component. The internodes are passive units with a linear resistive transmembrane current represented by a constant conductance for each membrane layer. The active compartments (nodes, CAIS, PAIS) were modelled with 10-fold Hodgkin Huxley ion channel kinetics at an adjusted temperature of 29 °C. The soma was modelled with Hodgkin Huxley ion channel kinetics and three myelin layers. For lengths of sections, electrical properties and the full set of differential equations the reader is referred to [5-7].

For each ANF we investigate 7 different electrodes: one is placed inside the ST 150µm away from PTerm (minDend). This position has no equivalent in the SV, since this first part of the ANF is in proximity to the SM not SV. The mid-dendritic electrode positions (midDend) in ST and SV are placed 150µm below and above the 2nd PN. The midScala electrode positions are at the centre of the biggest circle inside the respective scala. Another electrode position was placed as close as possible to the soma (minSoma). Thus, the midScala and minSoma positions do not have a fixed minimal distance to the ANF (Figure 1 right).

For each electrode 100µs monophasic pulses were tested for both polarities: cathodic (CAT) and anodic (ANO). The extracellular potential along the ANF is calculated via $V_{e,n}=\rho_e I_{el}/4\pi r_n$ where r_n is the distance to the *n*-th fiber section and $\rho_e=300\,\Omega cm$ the homogeneous extracellular resistivity. Simulations were performed with NEURON [8].

3 Results and Discussion

The calculated thresholds for all electrodes and intact, healthy target fibres are presented in Figure 1 at the left. At each electrode position the upper half portion of the symbol corresponds to the threshold for ANO stimulation, and the lower one to the CAT counterpart. For all ANFs the lowest thresholds are found for midDend positions (diamond electrodes): the ANO threshold is 42µA and 22µA for CAT

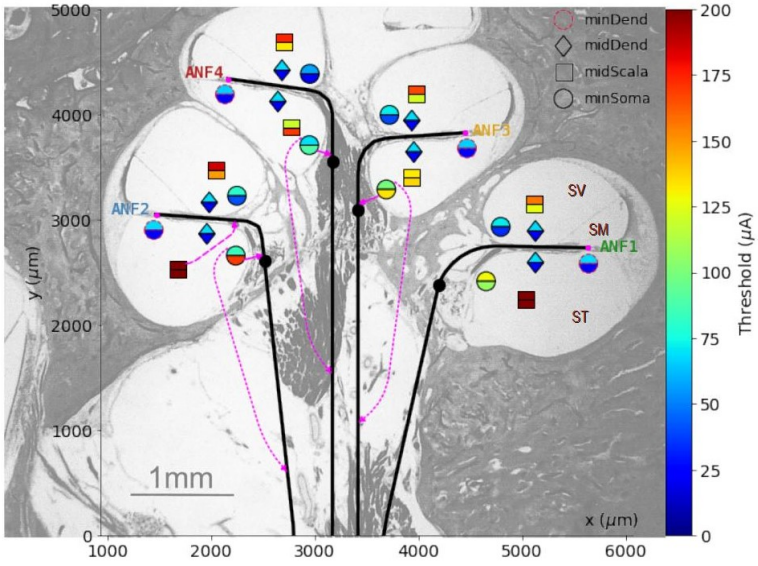

	ANF1		ANF2		ANF3		ANF4	
	minimum distance	soma distance	minimum distance	soma distance	minimum distance	soma distance	minimum distance	soma distance
ST								
minDend ○	150 PTerm	1459	150 PTerm	1107	150 PTerm	1205	150 PTerm	1217
midDend ◇	150 PN[2]	956	150 PN[2]	612	150 PN[2]	773	150 PN[2]	775
midScala □	502 PI[3]	848	510 PN[1]	841	386 PN[2]	608	375 PI[3]	516
minSoma ○	323 PI[5]	458	270 PAIS	281	273 PI[6]	337	231 PI[6]	271
SV								
midDend ◇	150 PN[2]	956	150 PN[2]	612	150 PN[2]	773	150 PN[2]	775
midScala □	413 PN[2]	1199	458 PN[2]	980	401 PI[2]	1237	423 PI[2]	1231
minSoma ○	189 PI[4]	812	231 PN[3]	674	224 PN[3]	956	153 PN[3]	860

Figure 1: (**left**) Four ANF pathways with soma position and corresponding electrodes in the human cochlea. Color-coded thresholds for ANO (top part of electrode) and CAT pulses (bottom part). Magenta dots mark the regular spike initiation sites at PTerm, magenta lines show exceptions. (**right**) Minimum electrode-fibre distance and electrode-soma distances [µm] for all ANFs and electrodes.

pulses, which shows little to no variation for different ANFs and is also the same for ST and SV electrodes. The minDend electrodes (red dashed circle electrodes) show similar CAT thresholds, and a slightly higher ANO threshold value of 67µA. In all of these cases the AP is initiated in PTerm (Figure 1: magenta dots) which is the easiest segment to excite due to the proximity to the active electrode and the lack of a preceding neighbour causing less axial current loss.

The highest threshold values are observed for midScala electrodes (rectangular electrodes), where the median ANO threshold is 170µA for both the ST and SV positions. Contrary to SV electrodes, the ST positions show a high threshold variance in different ANFs which is a consequence of the difference in electrode-fibre distances (Figure 1 right). CAT thresholds of midScala positions are always lower for SV electrodes with a median value of 129µA. Yet, for ST electrodes the median CAT threshold is increased to 189µA, i.e., the CAT threshold is only lower than the ANO value in ANF2 (see Figure 2 top). This case is also the only discrepancy when considering spike initiation sites: For all midScala electrodes and pulses of both polarities the AP always starts in PTerm, except for the ST positions and ANO stimulation of ANF2 (Figure 1: dashed magenta line).

For minSoma positions (black circle electrodes) the results predict varying spike initiation sites. For SV positions APs always starts in PTerm, because minimum electrode-fibre distance is registered for more peripheral segments of the ANF (Figure 1 right). The ST positions are closer to the central axon which has a larger diameter and thus is easier to excite than the thinner dendrite, i.e., for ANF2-ANF4 ANO pulses initiate the AP in the 3rd CN (Figure 1: dotted magenta lines) and the CAT pulses in PAIS (Figure 1: magenta lines). As a consequence, for ST minSoma electrodes the median ANO threshold of 91µA is lower than the median CAT threshold of 119µA. For SV positions this relationship is reversed and thresholds are again overall lower with less variation compared to ST equivalents: ANO median of 72µA and CAT median of 37µA.

The top part of Figure 2 summarizes the registered relationship between ANO and CAT thresholds, the percentage difference between thresholds is plotted for varying electrode positions for the four ANFs (coloured lines). Positive values indicate higher ANO thresholds and negative values higher CAT thresholds. The general trend for the healthy ANFs is lower CAT thresholds, which is in accordance with previously reported data in 3D inhomogeneous models [6].

The bottom part of Figure 2 depicts the direct comparison of equivalent electrode positions in ST and SV. For healthy ANFs with an intact dendrite the thresholds are generally lower for SV electrode positions compared to their equivalent ST position. The only irregularity occurs for midScala electrode positions and ANO stimulation of middle turn fibres ANF3 and ANF4, where a percentage decrease of -23% and -37% are registered respectively. Yet, for basal ANF1 and ANF2 the percentage increase of ST compared to SV midScala electrodes for ANO pulses are 26% and 78% respectively. The biggest advantage of SV positions compared to ST equivalents is found for CAT stimulation at minSoma positions where ST thresholds show over 100% increase compared to SV electrodes.

In completely degenerated ANFs which have lost the whole dendrite, most of the electrodes are much further away from the ANFs. The closest segment to the electrode in degenerated ANFs is always the soma (distances in Figure 1 right). As a result thresholds are much higher than for healthy ANFs, whereas the increase for ANO thresholds compared to CAT threshold is lower and ST electrodes show less threshold increase than SV electrodes because SV electrodes

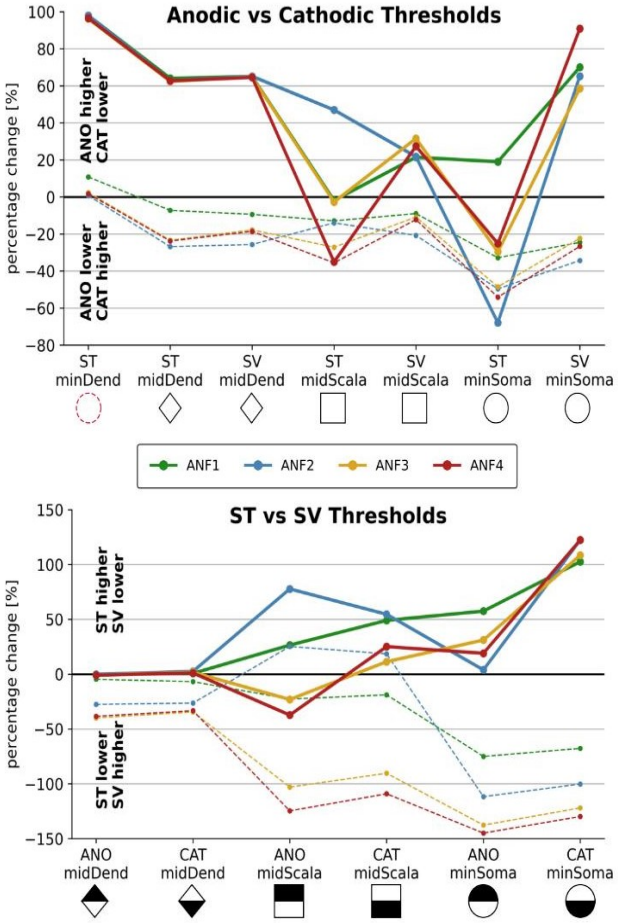

Figure 2: Percentage change of thresholds in each intact ANF (solid coloured lines) and the respective degenerated case (dotted lines) (**top**) Comparision of pulse polarity in all electrodes (**bottom**) Comparision of equivalent scala placement for all electrode positions and both pulse polarities.

are further away from the degenerated ANFs. The median increase of thresholds for degenerated ANFs compared to healthy ANFs and SV electrodes is 657% for ANO stimulation and 1757% for CAT. The highest increase is registered for the midDend positions, followed by minSoma electrodes and it is lowest for midScala electrodes. For ST electrodes these values are much lower when the minDend position is omitted from the statistic, i.e., the median threshold increase is 124% for ANO pulses and 243% for CAT pulses. Additionally, in the case of ST electrodes the threshold increase is higher for midScala electrodes than for minSoma positions, where thresholds are not significantly increased compared to healthy ANFs for both polarities. Specifically, for CAT pulses of the ST minSoma electrode the thresholds are almost the same for healthy and degenerated ANF2 due to similar electrode-fibre distance.

In the degenerated ANFs the spike initiation site always differs for all electrode positions when switching polarity, i.e., ANO stimulation favours initiation in one of the central nodes (the majority in the 5th and 6th CN), whereas CAT stimulation mostly excites the soma directly or the 1st CN. Consequently, ANO thresholds are almost always lower than CAT thresholds for degenerated ANFs (Figure 2 top thin lines) which is in accordance with simulation studies [6,9]. Furthermore, the advantage of SV electrodes is lost in the degenerated case and ST positions have generally lower threshold values. However, for basal ANFs the difference is less pronounced and SV midScala positions even outperform their ST counterparts for both stimulus polarities in ANF2 (Figure 2 bottom thin lines).

We also ran simulation for partially degenerated ANFs which have a dendrite of half the diameter and half the myelin sheets (data not shown). Threshold increase is much less severe, spike initiation sites remain almost unchanged and the relationship between ANO and CAT pulses is similar as is the superiority of SV electrodes. A deeper investigation like [9] should be performed to study different degrees of degeneration of ANFs which could help clinical decision making for the potential SV insertion of the CI. In summary, the presented simplistic 2D model is able to predict and replicate general trends. Yet, it cannot be ruled out that interesting detail is missed because of the specific spiralling pattern of 3D ANF pathways [6].

However, the biggest shortcoming of this study is the lack of inhomogeneity in the extracellular space and it is likely that the differences in resistivity of varying tissues have a strong effect on the induced V_e along the ANFs. Future studies based on a volume conductor model and finite element analysis shall clarify how much the results change. Specifically for basal ANFs and the clinically relevant midScala position thresholds for ST and SV electrodes remain comparable. The basal region of the ST is also heavily affected by ossification and since bone structures have a very high resistivity it cannot be ruled out that ST electrode thresholds will be significantly increased.

4 Conclusion

Our results confirm that CI electrodes placed in the SV are capable of eliciting the same neural response at comparable thresholds to ST electrodes. Future studies with a 3D volume conductor model shall obtain results for realistic ANF pathways, varying degeneration degrees and clarify the impact on the induced electric field of the inhomogeneous tissue resistivity, specifically due to ossification in ST.

Author Statement

This research was supported by the Austrian Science Fund (FWF): P36271-N. Authors state no conflict of interest.

References

[1] Zeng F-G. Celebrating the one millionth cochlear implant. JASA Express Lett 1 2022;2(7): 077201.

[2] Steenerson RL, Gary LB, Wynens MS. Scala vestibuli cochlear implantation for labyrinthine ossification. Am J Otol 1990;11(5): 360-363.

[3] Trudel M, Côté M, Philippon D, Simonyan D, Villemure-Poliquin N, Bussières R. Comparative Impacts of Scala Vestibuli Versus Scala Tympani Cochlear Implantation on Auditory Performances and Programming Parameters in Partially Ossified Cochleae. Otol Neurotol. 2018;39(6):700-6.

[4] Holzmeister C, Andrianakis A, Kiss P, Moser U, Graupp M. Scala vestibuli cochlear implant supported by 3D modeling of the inner ear. Wien Klin Wochenschr 2022;134: 243–248.

[5] Rattay F, Leao RN, Felix H. A model of the electrically excited human cochlear neuron. II. Influence of the three-dimensional cochlear structure on neural excitability. Hear Res 2001; 153 (1-2):64-79.

[6] Potrusil T, Heshmat A, Sajedi S, Wenger C, Chacko LJ, Glueckert R, et al. Finite element analysis and three-dimensional reconstruction of tonotopically aligned human auditory fiber pathways: A computational environment for modeling electrical stimulation by a cochlear implant based on micro-CT. Hear Res 2020;393: 108001.

[7] Rattay F. Basics of hearing theory and noise in cochlear implants. Chaos, Solitons & Fractals 2020;11(12), 1875-84.

[8] Carnevale NT, Hines ML. The NEURON Book. Cambridge, UK: Cambridge University Press, 2006

[9] Heshmat A., Sajedi S, Lejo JC, Fischer N, Schrott-Fischer A, Rattay F. Dendritic Degeneration of Human Auditory Nerve Fibers and Its Impact on the Spiking Pattern Under Regular Conditions and During Cochlear Implant Stimulation. Front Neurosci 2020;14.